Modelling ice mélange based on the viscous-plastic sea-ice rheology

Saskia Kahl[1], Carolin Mehlmann[1], and Dirk Notz[2]

[1]Institute of Analysis and Numerics, Otto-von-Guericke Universität, Magdeburg, Germany
[2]Center for Earth System Research and Sustainability (CEN), Institute of Oceanography, Universität Hamburg, Germany

Correspondence: Saskia Kahl (saskia.kahl@ovgu.de)

Abstract. Ice mélange, which is a mixture of sea ice, bergy bits and icebergs, can have a strong influence on the sea-ice–ocean interaction. So far, ice mélange is not represented in climate models as numerically efficient realizations are missing. This motivates the development of an ice-mélange model based on the viscous-plastic sea-ice rheology, which is currently the most commonly used material law for sea ice in climate models. Starting from the continuum mechanical formulation, we modify the rheology so that icebergs are represented by thick, highly compact pieces of sea ice. These compact pieces of sea ice are held together by a modified tensile strength in the material law. In this framework, the ice mélange is considered as one single fluid, where the icebergs are tracked by a volume in fluid method. Using idealized test cases, we demonstrate that the proposed changes in the material law are crucial to represent icebergs with the viscous-plastic rheology. Similar to the viscous-plastic sea-ice model, the ice-mélange model is highly nonlinear. Solving the model at the resolution needed to represent the typical size of icebergs in ice mélange (< 300 m) is therefore challenging. We show that the ice-mélange formulation can be approximated efficiently with a modified Newton method. Overall, the simple extension of the viscous-plastic sea-ice model is a promising path towards the integration of ice mélange in climate models.

1 Introduction

Fjords with marine terminating glaciers are commonly found in the polar regions, for example around Greenland. These fjord systems can be filled with sea ice into which icebergs calve, so that a mixture of sea ice, bergy bits and icebergs is formed: *ice mélange*. In winter, this granular material can build a compact ice cover that provides a backstress on the glacier front (Amundson et al., 2010). During spring, the ice mélange disintegrates. Observations show that the seasonal pattern of glaciers and ice mélange overlap, leading to the assumption that increased iceberg calving is related to the ice mélange decline in spring (Foga et al., 2014). To explain this finding, Howat et al. (2010) suggest that the ice mélange has a significant *buttressing effect* on the glacier front. The buttressing effect describes the equilibrium state in which ice mélange builds up enough resistance to suppress iceberg calving.

The possible influence of this potential buttressing effect of ice mélange on the glacier dynamics likely plays an important role in today's warming climate: Marine-terminating glaciers contribute to global sea level rise through melting, but also through releasing their freshwater storage through calving icebergs. The buttressing effect of the ice mélange might modify the time evolution of this latter contribution to sea-level rise. In addition, also the influence of ice mélange on the ocean circulation is an open research question (Martin and Adcroft, 2010; Enderlin and Hamilton, 2014).

To obtain insights into the potential impact of ice mélange on glacier calving and the underlying ocean circulation, numerical models are necessary. This is the more the case as observing ice mélange is difficult, due to the sparsity of satellite images (Cassotto et al., 2015). In general, there are two distinct approaches to include ice mélange into models: Either the

30 mélange is modelled explicitly, or its impact is parameterized. However, parameterizations can only cover some parts of the interaction between the ice mélange and the climate system, for example the buttressing effect (Schlemm and Levermann, 2021).

To study the interaction between the ocean, glaciers, the atmosphere and the ice mélange in more detail, the mélange needs to be modelled explicitly. There are two distinct approaches in the scientific literature for doing so: In the continuum approach,

35 the ice mélange is modelled as a single fluid (e.g. Seneca Lindsey and Dupont, 2012; Vaňková and Holland, 2017; Pollard et al., 2018). In contrast, in particle methods the ice mélange is expressed using discrete interacting particles, with single particles representing icebergs or sea-ice floes (e.g. Bassis and Jacobs, 2013; Åström et al., 2014; Peters et al., 2015; Robel, 2017; Burton et al., 2018). As ice mélange consists of many interacting small icebergs (< 300 m) (Dowdeswell et al., 1992), implementing the particle approach into climate models would be extremely challenging due to the enormous numerical costs.

40 This is the more the case as the particle models need a time step in the order of seconds to be numerically stable (Vaňková and Holland, 2017). In addition, it is currently unclear how a particle mélange model could be coupled to the commonly used continuum sea-ice formulation.

To avoid these difficulties, we here develop an ice-mélange model based on the continuum approach. In this approach, a mixture of fluids or of materials is seen a single material, whose density distribution in individual grid cells is modelled. This

45 implies that particles and their complex interactions do not have to be tracked individually. Using such approach, Vaňková and Holland (2017) propose a continuum formulation for ice mélange based on the captivating fluid sea-ice rheology introduced by Flato and Hibler (1992).

Most climate models, however, treat sea ice as a viscous-plastic material using the viscous-plastic (Hibler, 1979) or elastic-viscous-plastic (Hunke, 2001) sea-ice rheology. These rheologies are used in 30 out of the 33 global climate models of the

50 Climate Model Intercomparison Project 5 (CMIP5) (Stroeve et al., 2014). Furthermore, observations from Greenlands three most productive marine terminating glaciers (Jakobshavn Isbræ, Helheim and Kangerdlugssuaq Glacier) indicate that for granular materials such as ice mélange, constitutive relationships like the viscous-plastic flow are valid (Amundson and Burton, 2018). Thus, an inclusion of ice mélange into climate models via a modification of the viscous-plastic material law is a promising approach.

55 We here develop a model of ice mélange based on the viscous-plastic rheology, introducing a spatially varying strength parameterization. In our framework, icebergs are explicitly modeled via a volume in fluid method (Hirt and Nichols, 1982), as thick, highly concentrated pieces of sea ice. Also Vaňková and Holland (2017) represented icebergs as thick, compact bits of sea ice. However, in addition to our different choice of the underlying rheology, we also go beyond their study by formulating a modified Newton method to solve the ice-mélange model very efficiently.

60 The paper is structured as follows: Section 2 presents the ice-mélange model. The model is numerically evaluated in Section 3. We discuss our results in Section 4 and summarize our conclusions in Section 5.

2 Viscous-plastic ice-mélange model

Currently, most climate models represent sea ice as a viscous-plastic material by using either the classical viscous-plastic rheology (Hibler, 1979) or the elastic-viscous-plastic model modification (Hunke, 2001). In the following, we formulate an expansion of the viscous-plastic rheology that includes the representation of icebergs. These are modelled as part of the ice mélange by representing them as thicker and highly concentrated blocks of solid ice. To keep these thick and concentrated pieces of ice together in the ice-mélange formulation, we modify the tensile strength of the viscous-plastic law.

In the following, we first generally review the formulation of the governing equations and the viscous-plastic rheology, before modifying its strength parameterization in Section 2.3 to represent icebergs.

2.1 Momentum and conservation equation

The viscous-plastic ice-mélange model consists of three prognostic variables, as in the underlying viscous-plastic sea-ice model (Hibler, 1979): the ice mélange's thickness H, its concentration A within a specific grid cell, and horizontal velocity $\boldsymbol{v}$. The drift of the ice mélange is described by the two-dimensional momentum equation

$$m\partial_t \boldsymbol{v} = \operatorname{div}\boldsymbol{\sigma} + F, \tag{1}$$

where m is the mass per unit area and $\operatorname{div}\boldsymbol{\sigma}$ describes the two-dimensional symmetric stress tensor. The internal stresses are given by the material law described in Section 2.3. The remaining terms collected in F

$$F = F_C + F_H + \tau_{atm} + \tau_{\text{ocean}}(\boldsymbol{v}), \tag{2}$$

model the body forces acting on the ice mélange: the Coriolis force F_C, the surface height force F_H emerging from a potential surface tilt, and the atmospheric and oceanic stresses given by τ_{atm} and τ_{ocean}. These two drag terms (Coon, 1980) are expressed as

$$\tau_{atm} = C_{\text{atm}}\rho_{\text{atm}} \left\| \boldsymbol{v}_{\text{atm}} \right\|_2 (\boldsymbol{v}_{\text{atm}}), \tag{3}$$

$$\tau_{ocean}(\boldsymbol{v}) = C_{\text{ocean}}\rho_{\text{ocean}} \left\| \boldsymbol{v} - \boldsymbol{v}_{\text{ocean}} \right\|_2 (\boldsymbol{v} - \boldsymbol{v}_{\text{ocean}}), \tag{4}$$

where $\boldsymbol{v}_{\text{atm}}$ describes the wind velocity and $\boldsymbol{v}_{\text{ocean}}$ the ocean current. The corresponding densities are given by $\rho_{\text{atm}} = 1.3 \text{ kgm}^{-3}$ and $\rho_{\text{ocean}} = 1026 \text{ kgm}^{-1}$. The drag coefficients are $C_{\text{atm}} = 1.2 \times 10^{-3}$ and $C_{\text{ocean}} = 5.5 \times 10^{-3}$. Note that $\left\|\cdot\right\|_2$ is the Euclidean norm.

The advection of the ice-mélange thickness H and concentration A are calculated as

$$\partial_t H + \operatorname{div}(H\boldsymbol{v}) = S_{\text{H}},$$
$$\partial_t A + \operatorname{div}(A\boldsymbol{v}) = S_{\text{A}} \tag{5}$$

with $H \in [0, \infty)$ and $A \in [0, 1]$. Since we here focus on the description of ice-mélange dynamics, the thermodynamics processes expressed by the source terms are set to $S_{\text{H}} = S_{\text{A}} = 0$.

2.2 Viscous-plastic rheology

90

In the viscous-plastic model (Hibler, 1979), the states of the stress $\boldsymbol{\sigma}$ are described by an elliptic yield curve of the form

$$F(\tilde{\boldsymbol{\sigma}}_1, \tilde{\boldsymbol{\sigma}}_2) = \left(\frac{\tilde{\boldsymbol{\sigma}}_1 + \tilde{\boldsymbol{\sigma}}_2 + P}{P}\right)^2 + \left(\frac{\tilde{\boldsymbol{\sigma}}_1 - \tilde{\boldsymbol{\sigma}}_2}{P}e\right)^2 - 1 = 0. \tag{6}$$

This curve is expressed in the principal components of the stress tensor $\boldsymbol{\sigma}$

$$\tilde{\boldsymbol{\sigma}}_1 = \frac{\boldsymbol{\sigma}_{11} + \boldsymbol{\sigma}_{22}}{2} + \sqrt{\left(\frac{\boldsymbol{\sigma}_{11} - \boldsymbol{\sigma}_{22}}{2}\right)^2 + \boldsymbol{\sigma}_{12}^2},$$

$$\tilde{\boldsymbol{\sigma}}_2 = \frac{\boldsymbol{\sigma}_{11} + \boldsymbol{\sigma}_{22}}{2} - \sqrt{\left(\frac{\boldsymbol{\sigma}_{11} - \boldsymbol{\sigma}_{22}}{2}\right)^2 + \boldsymbol{\sigma}_{12}^2}. \tag{7}$$

95   The minor axis of the ellipse has a ratio $e = 2$, whereas the length of the major axis is given by the sea-ice strength

$$P = P^\star H \exp(-C(1 - A)), \tag{8}$$

with strength parameter $P^\star = 27.5 \times 10^3 \text{ Nm}^{-2}$ and $C = 20$. A visualization of the yield curve is given in Figure 1 (blue line). As there are no stress states on the yield curve with $(\tilde{\boldsymbol{\sigma}}_1, \tilde{\boldsymbol{\sigma}}_2) > 0$, sea ice has almost no tensile strength (no resistance to divergence) (Leppäranta, 2011). The stress states are related to the strain rates

100   $$\dot{\boldsymbol{\epsilon}}_{ij} = \frac{1}{2}\left\{\partial_{\mathbf{x}_j}\boldsymbol{v}_i + \partial_{\mathbf{x}_i}\boldsymbol{v}_j\right\}, \tag{9}$$

by the constitutive law (Hibler, 1979)

$$\boldsymbol{\sigma}_{ij} = 2\eta\dot{\boldsymbol{\epsilon}}_{ij} + (\zeta - \eta)(\dot{\boldsymbol{\epsilon}}_{11} + \dot{\boldsymbol{\epsilon}}_{22})\delta_{ij} - \frac{P}{2}\delta_{ij}, \tag{10}$$

where δ_{ij} is the Kronecker symbol. The nonlinear shear ζ and bulk viscosity η are chosen as

$$\eta = e^{-2}\zeta, \quad \zeta = \frac{P}{2\Delta(\dot{\boldsymbol{\epsilon}})}. \tag{11}$$

105   In case of the plastic regime, $\Delta(\dot{\boldsymbol{\epsilon}})$ is chosen as $\Delta_P(\dot{\boldsymbol{\epsilon}})$, which is defined as

$$\Delta_P(\dot{\boldsymbol{\epsilon}}) = \sqrt{(\dot{\boldsymbol{\epsilon}}_{11}^2 + \dot{\boldsymbol{\epsilon}}_{22}^2)(1 + e^{-2}) + 4e^{-2}\dot{\boldsymbol{\epsilon}}_{12}^2 + 2\dot{\boldsymbol{\epsilon}}_{11}\dot{\boldsymbol{\epsilon}}_{22}(1 - e^{-2})}. \tag{12}$$

The viscous closure is given as

$$\Delta_{\min}(\dot{\boldsymbol{\epsilon}}) = 2 \times 10^{-9}. \tag{13}$$

To guarantee a smooth transition between the viscous and the plastic regime we follow Kreyscher et al. (2000) and choose

110   $$\Delta(\dot{\boldsymbol{\epsilon}}) = \sqrt{\Delta_P(\dot{\boldsymbol{\epsilon}})^2 + \Delta_{\min}^2}. \tag{14}$$

Such smooth transition is essential for the design of efficient implicit solvers.
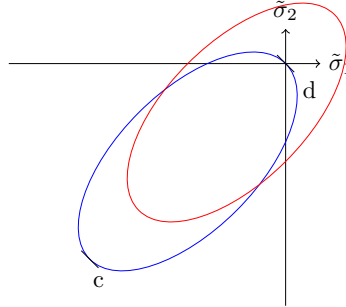
Figure 1. Two-dimensional yield curve in principal stress space without (blue) and with (red) tensile strength. Pure divergence d is in the origin of the graph, pure convergence is obtained in c. $\tilde{\boldsymbol{\sigma}}_1$ and $\tilde{\boldsymbol{\sigma}}_2$ are the principal components of the stress tensor $\boldsymbol{\sigma}$ (see Eq. (10)).

2.3 Strength parameterization

The absence of tensile strength in the original model is apparent from the fact that the yield curve of the viscous-plastic rheology does not contain combinations of $(\tilde{\boldsymbol{\sigma}}_1, \tilde{\boldsymbol{\sigma}}_2) > 0$ (see blue curve in Figure 1). A tensile strength has been introduced into this model for example by König and Holland (2010) to model landfast ice, or in the ice-mélange model based on a cavitating-fluid rheology (Vaňková and Holland, 2017). Vaňková and Holland (2017) suggest a parameterization of the tensile and shear strength to represent icebergs in the continuum formulation. Similar to this approach, we introduce a tensile strength into the standard viscous-plastic sea-ice rheology to model icebergs. This tensile strength is supposed to lead to a resistance to divergence in the presence of icebergs.

By including the tensile strength, the elliptic yield curve is shifted into the first quadrant (red curve in Figure 1). The new center of the ellipse is given by $\left(-\frac{P-T}{2}, -\frac{P-T}{2} \right)$, with the maximum tensile strength T. Both P and T are positive numbers. Thus, the modified elliptic yield curve is given by

$$F\left(\tilde{\boldsymbol{\sigma}}_1, \tilde{\boldsymbol{\sigma}}_2\right) = \left(\frac{\tilde{\boldsymbol{\sigma}}_1 + \tilde{\boldsymbol{\sigma}}_2 + P - T}{P + T} \right)^2 + \left(\frac{\tilde{\boldsymbol{\sigma}}_1 - \tilde{\boldsymbol{\sigma}}_2}{P + T} e \right)^2 - 1 = 0, \tag{15}$$

with the elliptic ratio e. For $T = 0$ (no tensile strength), the elliptic yield curve is equivalent to the ellipse of the viscous-plastic sea-ice rheology (see Eq. (6)).

The relation between the stress tensor and the strain rates for the shifted yield curve is derived by assuming a normal flow rule

$$\dot{\boldsymbol{\epsilon}}_{ij} = \gamma \frac{\partial F(\boldsymbol{\sigma}_{11}, \boldsymbol{\sigma}_{22}, \boldsymbol{\sigma}_{12}, \boldsymbol{\sigma}_{21})}{\partial \boldsymbol{\sigma}_{ij}}, \tag{16}$$

with $\gamma > 0$. This leads to the modified rheology

$$\boldsymbol{\sigma}_{ij} = 2\eta \dot{\boldsymbol{\epsilon}}_{ij} + (\zeta - \eta)\left(\dot{\boldsymbol{\epsilon}}_{11} + \dot{\boldsymbol{\epsilon}}_{22}\right) \delta_{ij} - \frac{P - T}{2} \delta_{ij}, \tag{17}$$

with the bulk and shear viscosities

$$\zeta = \frac{P + T}{2\Delta}, \quad \eta = \frac{\zeta}{e^2} = \frac{P + T}{2\Delta e^2}. \tag{18}$$

Following König and Holland (2010), we define the tensile strength T relative to the compressive strength

$$T = P^\star H \Phi. \tag{19}$$

135 According to the volume in fluid method (Hirt and Nichols, 1982) the indicator function Φ is given as

$$\Phi = \begin{cases} 0 \text{ if } \phi \leq c & \text{for sea ice,} \\ 1 \text{ if } \phi > c & \text{for icebergs.} \end{cases} \tag{20}$$

The threshold ϕ is transported via

$$\partial_t \phi + \mathrm{div}(\phi \boldsymbol{v}) = 0. \tag{21}$$

For $\phi = 0$ (e.g $T = 0$), the equation (17) reduces to the standard viscous-plastic model.

140 2.4 Numerical discretization

The ice-mélange model is implemented in the academic software library Gascoigne (Braack et al., 2021). We use a splitting-in-time method to solve the coupled system of equations that express the ice mélange. First, we approximate the solution of the transport equations (5) and (21). With the updated tracers, we then compute the solution of the momentum equation (Eq. 1).

The transport equations are solved with a Flux-Corrected Taylor-Galerkin scheme. More details on the implementation can 145 be found in Mehlmann (2019). The momentum equation is discretized with the implicit Euler method. This choice is motivated by the fact that an explicit discretization of the viscous-plastic sea-ice model requires a time step of $1\,\mathrm{s}$ on a grid with size $100\,\mathrm{km} \times 100\,\mathrm{km}$ (Ip et al., 1991). We expect similar constraints for the ice-mélange model, because its rheology is based on the viscous-plastic sea-ice model.

For our choice of an implicit temporal discretization, a nonlinear system of differential equations needs to be solved in every 150 time step. We suggest to use a modified Newton method for this solution. This choice arises from the following findings: For the time discretized equations we can proof that the Jacobian of the momentum equation in its weak formulation is positive definite. Therefore, the properly damped Newton scheme converges towards the analytical solution of the time discretized equations (Mehlmann and Richter, 2017). Essential for this proof is the use of the smooth closure between the viscous and the plastic regime, Eq. (14). As in the case of the viscous-plastic model, the Jacobian of the ice-mélange model can be split into 155 a positive and negative semi-definite part. This motivates the use of a modified Newton solver to approximate the momentum equation of the ice-mélange model. The properties of the Jacobian can be proven analogous to Mehlmann and Richter (2017) taking into account that $P + T \leq 0$. The idea of the modified Newton solver is to damp the negative-semidefinite parts of the Jacobian once the convergence of the solver worsens. This technique improves the performance of the modified Newton method substantially.
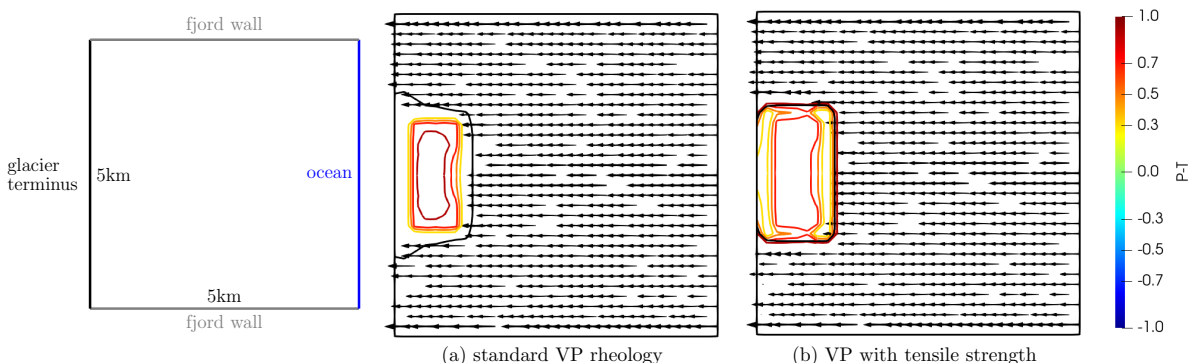
Figure 2. Visualization of the normalised internal pressure p (contour lines) and the ice-mélange velocity (black arrows) for a test case in which an iceberg (thick black contour line) is pushed against the glacier terminus (left boundary) by a constant wind ($\boldsymbol{v}_{\mathrm{atm}} = 20\,\mathrm{ms}^{-1}$). The panels denote the results for (a) the standard viscous-plastic rheology and (b) for the viscous-plastic rheology with tensile strengths. Both snapshots show the simulation result after 1 h.

3 Numerical validation

The proposed model is tested in three idealized test cases. The first three test cases are designed such that the behavior of the ice mélange is tested under tensile (Section 3.1), compressive (Section 3.2) and shear (Section 3.3) strength. This is necessary because ice mélange is exposed to extreme forcing, especially during calving events. While the glacier pushes the ice mélange out of the fjord, tensile and compressive strengths play a major role in the center of the fjord. Along the coast, the ice mélange is blocked so that shear stress dominates (Burton et al., 2018). For the stake of simplicity the ocean forcing is neglected ($\boldsymbol{v}_{\mathrm{ocean}} = 0\,\mathrm{ms}^{-1}$) for all test cases.

3.1 Iceberg pushed against a wall

The first test case is similar to the one used by Vaňková and Holland (2017). The domain is given by an area of the size $5\,\mathrm{km} \times 5\,\mathrm{km}$, see left plot in Figure 2. All boundaries except the exit to the ocean (right boundary) use Dirichlet boundary conditions ($\boldsymbol{v} = 0$). The upper and lower boundaries represent the coast lines, while the boundary on the left represents the glacier terminus. We place a $1\,\mathrm{km} \times 2\,\mathrm{km}$ large iceberg in front of the glacier wall. A grid cells size of $110\,\mathrm{m}$ is used. The iceberg is a $10\,\mathrm{m}$ thick compact block of ice with a concentration of 1. The left half ($< 2.5\,\mathrm{km}$) of the domain is filled with $0.1\,\mathrm{m}$ thick sea ice with a concentration of 0.1. The iceberg is pushed against the glacier terminus through a constant wind $\boldsymbol{v}_{\mathrm{atm}} = 20\,\mathrm{ms}^{-1}$.

The simulation is run for 1 h. When comparing the standard viscous-plastic rheology and the modified material law (Figure 2), we find that for the standard viscous-plastic rheology, the iceberg and the sea ice move towards the glacier and accumulate in front of the glacier terminus. This is visible by the thick black line shown in Figure 2(a), which visualizes the iceberg's contour. With the proposed modification, the iceberg is able to keep its rectangular shape throughout the simulation (see Fig-
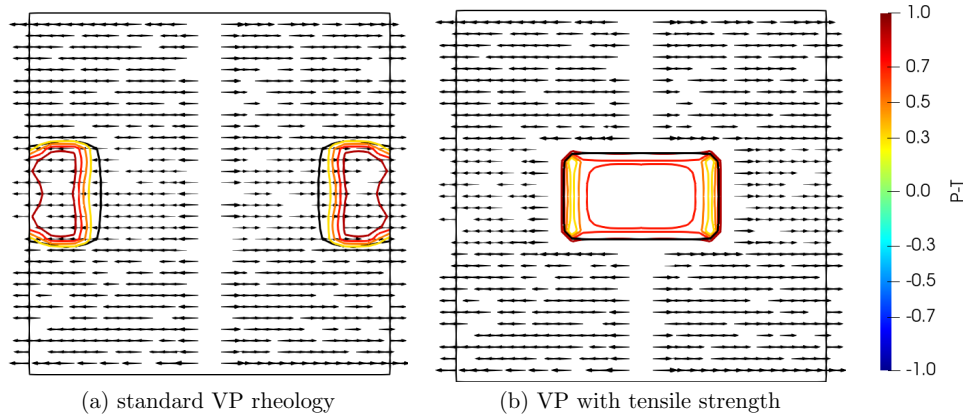
Figure 3. The iceberg (thick black contour line) is placed under a divergent wind field. The normalised internal pressure p is visualized by the contour lines and the ice-mélange velocity by the black arrows. The panels denote the results for (a) the standard viscous-plastic rheology and (b) for the viscous-plastic rheology with tensile strengths. Both snapshots show the simulation after 3 h. The thick black line shows the iceberg contour.

ure 2(b)). This test case shows that in our modified VP rheology, the iceberg can withstand the compression, initiated by the wind forcing.

3.2 Iceberg under a divergent wind field

We consider a 5 km × 5 km large channel with a divergent wind field

$$\boldsymbol{v}_{\text{atm}} = \begin{cases} 15 \, \text{ms}^{-1} & x > 2.5 \, \text{km}, \\ -15 \, \text{ms}^{-1} & x < 2.5 \, \text{km}. \end{cases} \tag{22}$$

The 10 m thick iceberg with a concentration of 1 is placed in the middle of the domain. The whole domain is filled with sea ice whose concentration is 0.1 and whose thickness is 0.1 m. Using the standard viscous-plastic rheology, the iceberg is torn apart after 3 h (see Figure 3(a)). With additional tensile strength the iceberg keeps its form (see Figure 3(b)). The surrounding sea ice is still transported in wind direction. This test case shows in particular that the iceberg maintains its shape even under diverging wind conditions at the location of the iceberg.

3.3 Two travelling icebergs

After testing whether the modification leads to shape preservation, it is crucial to test the interaction of icebergs travelling through sea ice. We consider the same channel domain as used in the second test case (Section 3.2). The 0.1 compact and 0.1 m thick sea ice fills the whole domain, in which two 1 km × 1 km icebergs are placed. The two 10 m thick icebergs have a concentration of 1. The icebergs are placed opposite each other in such a way that they can be transported past each other. The

(a) standard VP rheology   (b) VP with tensile strength
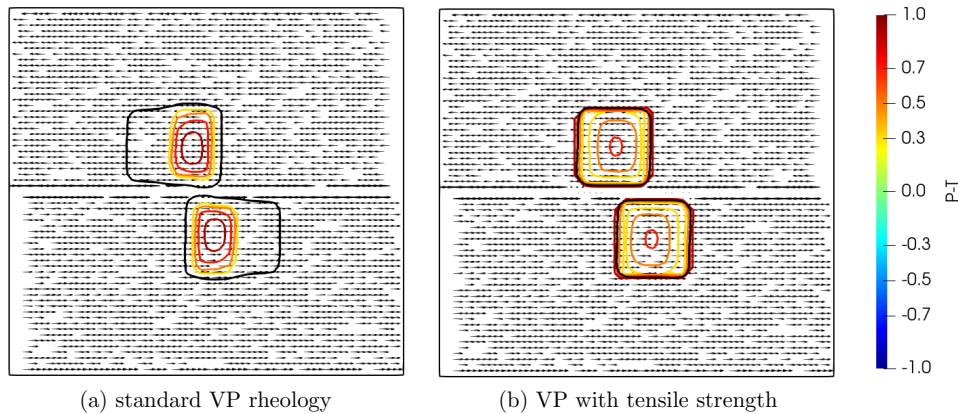
Figure 4. Two icebergs are transported past each other with a constant wind field ($\boldsymbol{v}_{\mathrm{atm}} = \pm\, 10\ \mathrm{ms}^{-1}$). The normalised internal pressure p is visualized by the contour lines and the ice-mélange velocity by the black arrows. Both snapshots show the simulation after 3 h. The thick black line shows the iceberg contour.

icebergs are forced by the following wind field:

$$
195 \quad \boldsymbol{v}_{\mathrm{atm}} = \begin{cases} 10\ \mathrm{ms}^{-1} & y < 2.5\ \mathrm{km}, \\ -10\ \mathrm{ms}^{-1} & y > 2.5\ \mathrm{km}. \end{cases} \tag{23}
$$

Figure 4(a) visualizes the test case using the viscous-plastic rheology. Without the tensile strength the icebergs diffuse. With included tensile strength (see Figure 4(b)) the icebergs keep their form and maintain their initial thickness of 10 m.

3.4 Solver performance

Besides modelling ice mélange, we also address the question of how the momentum equation of the ice-mélange model can be
200 solved efficiently. Vaňková and Holland (2017) formulated the need of efficient solvers for their ice-mélange model based on the cavitating-fluid rheology. The authors used a Picard-type solver to approximate the solution and noted that the use of their mélange formulation in climate models is "conditioned up to the development of an efficient numerical scheme" (Vaňková and Holland, 2017). To solve our ice-mélange model, we compare a Picard, Newton and modified Newton solver (Mehlmann and Richter, 2017) for the last test case (Section 3.3) as it is the most difficult one of the three setups.

205 Figure 5 compares the solver iterations per time step. The solver iterations per time step are limited to 100. The time step is considered as converged if the solver reaches the threshold (relative residual of 10^{-4} or global tolerance of 10^{-13}) within 100 iterations. The Picard solver fails in 19 out of 50 time steps. The standard Newton solver does not converge for 8 out of 50 time steps, while the modified Newton solver converges for all time steps. On average the Picard, Newton and modified Newton solver apply $48.26, 47.8$ and 27.38 iterations per time step, respectively. Thus, the modified Newton method reduces
210 the number of necessary iterations by 20 (40 %). This shows that the modified Newton method is more robust and efficient than the standard Newton solver and a Picard iteration.
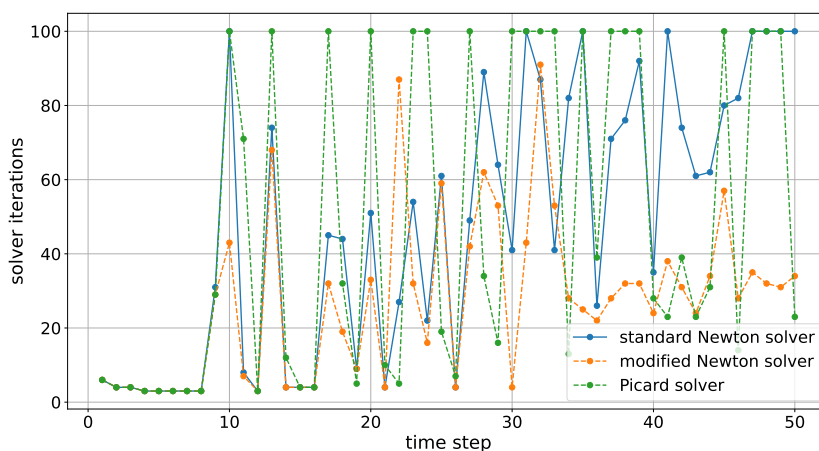
Figure 5. Solver iterations per time step for the third test case in which two icebergs are transported past each other with a constant wind field.
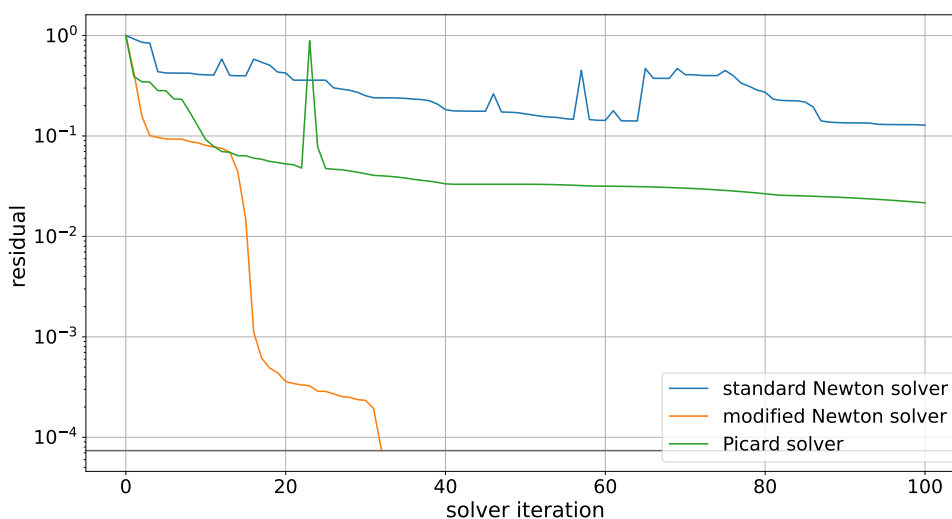
Figure 6. Residual reduction of the nonlinear solver during the 48th time step. The grey line indicates the threshold (relative residual of 10^{-4}) that has to be reached for a converging solution for each time step. The y-axis is plotted on a logarithmic scale.

Figure 6 shows one example of how the residual decreases per iteration during the 48th time step for each of the three solvers. The relative residual (grey line) is visualized in Figure 6. Out of the three solvers, only the modified Newton solver

converges. The standard Newton solver and Picard solver do not reach the threshold within 100 iterations. During the first few iterations, the Picard and modified Newton solver have a similar approximation behavior. The standard Newton solver converges the slowest. In the Picard solver, after 21 iterations with a decreasing residual, the residual of this solver suddenly shows a clear peak. Afterwards, the residual continues to decrease, but only very slowly. In contrast, our modified Newton solver converges after 32 iterations.

4 Discussion

The results from Section 3 show that the modification of the rheology is crucial to represent icebergs in the viscous-plastic model. Due to the modification of the strength parameter the motion of the ice mélange is close to a rigid body in the iceberg area. For simplicity, we have represented iceberg as rectangles. However, this choice has several disadvantages: The representation results in a uniform iceberg thickness, which may lead to a coarse approximation of the forces in the ice mélange. Furthermore, the volume-in-fluid method cannot represent the corners of the rectangles exactly such that the corners are easily smoothed out by the advection scheme. We therefore recommend to approximate the icebergs by other geometric objects such as cylinders, whose shape is easier to conserve.

Besides that, higher order approaches, such as discontinuous Galerkin methods, would also contribute to a more accurate representation of the icebergs. Another possibility to address the shortcoming of the volume-in-fluid method would be the usage of a particle-in-cell approach where the tracers are represented by particles.

To solve the ice-mélange model we presented an efficient Newton method. So far, only few models, e.g MITgcm, provide Newton schemes. Most climate model realize the viscous-plastic material by the elastic-viscous-plastic (EVP) formulation (Hunke, 2001). An inclusion of the strength parameterization into the elastic-viscous-plastic framework is straight forward. To ensure an efficient treatment, we recommend a realization of the ice-mélange model within the mEVP solver, which efficiently approximates EVP solutions (Koldunov et al., 2019).

Another assumption that could be relaxed in our mélange model is the usage of uniform drag coefficients for ocean and air. Instead, different values for sea ice and icebergs could be applied. The effect of drag on the iceberg sidewalls would need to be considered in this context. Additionally, including thermodynamics requires to change the mélange strength by melting or freezing and could be achieved by applying different melting coefficients for sea ice and icebergs.

5 Conclusions

We present an ice-mélange model based on a modification of the continuum viscous-plastic rheology, which is currently the most used material law for sea ice in climate models. The simple extension of the viscous-plastic sea-ice model makes it straight forward to include the ice-mélange model into a climate model.

Icebergs are introduced into the viscous-plastic rheology by a strength parameterization. The tensile strength parameterization is used in order to prevent icebergs from diffusing. Icebergs are represented by large, thick and compact pieces of ice,
245   tracked by the volume-in-fluid method (Eq. (21)) (Hirt and Nichols, 1982).

The usefulness and stability of the model is demonstrated using idealized examples. The setups shows that the icebergs maintain their shape under high pressure or difficult wind conditions. Likewise, we demonstrate that icebergs can also interact while maintaining their shape. These examples highlight situations where this modelling framework is beneficial. These are setups where the sea-ice cover is dense and the geometry of the fjord is complex such that sea-ice–iceberg interactions are
250   important.

To apply our ice-mélange formulation the grid resolution needs to be high enough to be able to capture icebergs. Therefore solving the ice-mélange model is challenging. Vaňková and Holland (2017) already formulated the need of efficient solvers for their ice-mélange model based on the cavitating-fluid rheology. To address this issue we suggest the usage of a modified Newton solver, which is more robust and efficient than a standard Newton formulation and a Picard solver.

255   *Code and data availability.* The model code used for the numerical examples are freely available from https://doi.org/10.5281/zenodo.7767470. The source code of Gascoigne is available to individuals (https://gascoigne.math.uni-magdeburg.de/index.php?show=downloadinstallation).

Author contributions. Saskia Kahl worked on the implementation. All the authors contributed to writing and discussion.

Competing interests. The authors declare that they have no conflict of interest.

Acknowledgements. CM acknoweledges funding by the Deutsche Forschungsgemeinschaft (DFG, German Research Foundation) - Project
260   number 463061012. DN acknowledges funding by the DFG under Germany's Excellence Strategy - EXC 2037 'CLICCS - Climate, Climatic Change, and Society' - Project Number: 390683824.

References

Amundson, J. M. and Burton, J. C.: Quasi-static granular flow of ice mélange, J. Geo. Res., 123, 2243–2267, https://doi.org/10.1029/2018JF004685, 2018.

265 Amundson, J. M., Fahnestock, M., Truffer, M., Brown, J., Lüthi, M. P., and Motyka, R. J.: Ice mélange dynamics and implications for terminus stability, Jakobshavn Isbræ, Greenland, J. Geophys. Res., 115, F01 005, https://doi.org/10.1029/2009JF001405, 2010.

Bassis, J. and Jacobs, S.: Diverse calving patterns linked to glacier geometry, Nat. Geosci., 6, 833–836, https://doi.org/10.1038/ngeo1887, 2013.

Braack, M., Becker, R., Meidner, D., Richter, T., and Vexler, B.: The Finite Element Toolkit Gascoigne, https://doi.org/10.5281/ZENODO.5574969, www.gascoigne.de, 2021.

270 Burton, J. C., Amundson, J. M., Cassottoc, R., Kuod, C.-C., and Dennin, M.: Quantifying flow and stress in ice mélange, the world's largest granular material, P. Natl. A. Sci., 115, 5105–5110, https://doi.org/10.1073/pnas.1715136115, 2018.

Cassotto, R., Fahnestock, M., Amundson, J. M., Truffer, M., and Joughin, I.: Seasonal and interannual variations in ice melange and its impact on terminus stability, Jakobshavn Isbræ, Greenland, J. Glaciol., 61, 76–88, https://doi.org/10.3189/2015JoG13J235, 2015.

275 Coon, M. D.: A review of AIDJEX modeling. In Sea Ice Processes and Models: Symposium Proceedings, University of Washington Press, Seattle, 1980.

Dowdeswell, J. A., Whittington, R. J., and Hodgkins, R.: The Sizes, Frequencies, and Freeboards of East Greenland Icebergs Observed Using Ship Radar and Sextant, J Geophys. Res., 97, 3515–3528, https://doi.org/10.1029/91JC02821, 1992.

Enderlin, E. M. and Hamilton, G. S.: Estimates of iceberg submarine melting from high-resolution digital elevation models: Application to
280 Sermilik Fjord, East Greenland, J. Glaciol., 60, 1084—1092, https://doi.org/10.3189/2014JoG14J085, 2014.

Flato, G. M. and Hibler, W. D.: Modelling Pack Ice as a Cavitating Fluid, J. Phys. Oceanogr., https://doi.org/0.1175/1520-0485(1992)022<0626:MPIAAC>2.0.CO;2, 1992.

Foga, S., Stearns, L. A., and van der Veen, C.: Application of Satellite Remote Sensing Techniques to Quantify Terminus and Ice Mélange Behavior at Helheim Glacier, East Greenland, Marine Technology Society Journal, 48(5), 81–91, https://doi.org/10.4031/MTSJ.48.5.3,
285 2014.

Hibler, W. D.: A Dynamic Thermodynamic Sea Ice Model, J. Phys. Oceanogr., 9, 815–846, https://doi.org/10.1175/1520-0485(1979)009<0815:ADTSIM>2.0.CO;2, 1979.

Hirt, C. W. and Nichols, B. D.: Volume of Fluid (VOF) Method for the Dynamics of Free Boundaries, Journals of Computational Physics, 39, 201–225, https://doi.org/10.1016/0021-9991(81)90145-5, 1982.

290 Howat, I. M., Box, J. E., Ahn, Y., Herrington, A., and McFadden, E. M.: Seasonal variability in the dynamics of marine-terminating outlet glaciers in Greenland, J. Glaciol., 56, 601–613, https://doi.org/10.3189/002214310793146232, 2010.

Hunke, E.: Viscous-Plastic Sea Ice Dynamics with the EVP Model: Linearization Issues, Journal of Computational Physics, 170, 18–38, https://doi.org/10.1006/jcph.2001.6710, 2001.

Ip, C. F., Hibler, W. D., and Flato, G. M.: On the effect of rheology on seasonal sea-ice simulations, Ann. Glaciol., 15, 17–25,
295 https://doi.org/10.3189/1991AoG15-1-17-25, 1991.

Koldunov, N., S.Danilov, Sidorenko, D., Hutter, N., Losch, M., Goessling, H., Rakowsky, N., Scholz, P., Sein, D., Wang, Q., and Jung, T.: Fast EVP Solutions in a High-Resolution Sea Ice Model, Journal of Advances in Modeling Earth Systems, 11, 1269–1284, https://doi.org/https://doi.org/10.1029/2018MS001485, 2019.

Kreyscher, M., Harder, M., Lemke, P., and Flato, G. M.: Results of the Sea Ice Model Intercomparison Project: Evaluation of sea ice rheology
300   schemes for use in climate simulations, J Geophys. Res.-Oceans, 105, 11 299–11 320, https://doi.org/10.1029/1999JC000016, 2000.

König, B. C. and Holland, D. M.: Modeling landfast sea ice by adding tensile strength, J. Phys. Oceanogr., 40, 185–198,
https://doi.org/10.1175/2009JPO4105.1, 2010.

Leppäranta, M.: The drift of Sea Ice, Springer-Verlag Berlin Heidelberg, 2011.

Martin, T. and Adcroft, A.: Parameterizing the fresh-water flux from land ice to ocean with interactive icebergs in a coupled climate model,
305   Ocean Model., 34, 111–124, https://doi.org/10.1016/j.ocemod.2010.05.001, 2010.

Mehlmann, C.: Efficient numerical methods to solve the viscous-plastic sea ice model at high resolutions, Ph.D. thesis, Otto-von-Guericke-
Universität Magdeburg, 2019.

Mehlmann, C. and Richter, T.: A modified global Newton solver for viscous-plastic sea ice models, Ocean Model., 116, 96–107,
https://doi.org/10.1016/j.ocemod.2017.06.001, 2017.

310 Peters, I. R., Amundson, J. M., Cassotto, R., Fahnestock, M., Darnell, K. N., Truffer, M., and Zhang, W. W.: Dynamic jamming of iceberg-
choked fjords, Geophys. Res. Lett., 42, 1122–1129, https://doi.org/10.1002/2014GL062715, 2015.

Pollard, D., DeConto, R. M., and Alley, R. B.: A continuum model (PSUMEL1) of ice mélange and its role during retreat of the Antarctic
Ice Sheet, Geosci. Model Dev., 11, 5149–5172, https://doi.org/10.5194/gmd-11-5149-2018, 2018.

Robel, A.: Thinning sea ice weakens buttressing force of iceberg mélange and promotes calving, Nat. Commun., p. 7,
315   https://doi.org/10.1038/ncomms14596, 2017.

Schlemm, T. and Levermann, A.: A simple parametrization of mélange buttressing for calving glaciers, The Cryosphere, 15, 531–545,
https://doi.org/10.5194/tc-15-531-2021, 2021.

Seneca Lindsey, D. and Dupont, T. K.: Mechanical effect of mélange-induced buttressing on embayment-terminating glacier dynamics, The
Cryosphere Discussions, 6, 4123–4136, https://doi.org/10.5194/tcd-6-4123-2012, 2012.

320 Stroeve, J., Barrett, A., Serreze, M., and Schweiger, A.: Using records from submarine, aircraft and satellites to evaluate climate model
simulations of Arctic sea ice thickness, The Cryosphere, 8, 1839–1854, https://doi.org/10.5194/tc-8-1839-2014, 2014.

Vaňková, I. and Holland, D.: A Model of Icebergs and Sea Ice in a Joint Continuum Framework, J Geophys. Res.-Oceans, 122, 9110–9125,
https://doi.org/10.1002/2017JC013012, 2017.

Åström, J. A., Vallot, D., Schäfer, M., Welty, E. Z., O'Neel, S., Bartholomaus, T. C., Liu, Y., Riikilä, T. I. an Zwinger, T., Timonen, J.,
325   and Moore, J.: Termini of calving glaciers as self-organized critical systems, Nat. Geosci., 7, 874–878, https://doi.org/10.1038/ngeo2290,
2014.